




Article

Mesoporous Organo-Silica Supported Chromium Oxide Catalyst for Oxidative Dehydrogenation of Ethane to Ethylene with CO₂

Abdulrhman S. Al-Awadi ¹, Ahmed Mohamed El-Toni ^{2,*}, Joselito P. Labis ², Aslam Khan ² , Hamid Ghaithan ³ , Attiyah A. Al-Zahrani ¹, Ahmed E. Abasaheed ¹  and Saeed M. Al-Zahrani ¹

¹ Chemical Engineering Department, King Saud University, Riyadh 11421, Saudi Arabia; alawadi@ksu.edu.sa (A.S.A.-A.); aazz@ksu.edu.sa (A.A.A.-Z.); abasaheed@ksu.edu.sa (A.E.A.); szahrani@ksu.edu.sa (S.M.A.-Z.)

² King Abdullah Institute for Nanotechnology, King Saud University, Riyadh 11451, Saudi Arabia; jlabis@ksu.edu.sa (J.P.L.); aslamkhan@ksu.edu.sa (A.K.)

³ Department of Physics, College of Science, King Saud University, Riyadh 11451, Saudi Arabia; hghaithan@ksu.edu.sa

* Correspondence: aamohammad@ksu.edu.sa; Tel.: +966-546194517

Abstract: Chromium oxide supported on mesoporous organo-silica (MOS) was synthesized with different Cr loading by an incipient method. The catalytic performance of a Cr(x)/MOS catalyst for CO₂-based ethane dehydrogenation was investigated. The synthesized catalysts were characterized by XRD, BET, TEM, SEM, XPS, FTIR, and UV-Vis DR measurements. The textural properties of the prepared samples showed that the mesoporous nature of MOS sample was not disturbed by chromium impregnation. Among the prepared samples, Cr(8)/MOS catalyst exhibited good distribution of chromium species along with superior concentration of Cr⁶⁺ and the highest recorded Cr⁶⁺/Cr³⁺ ratio. The results revealed that the superior catalytic performance was reached at Cr(8)/MOS, with 50.4% and 90.1% of ethane conversion and ethylene selectivity, respectively. The catalytic activity decreased slowly over reaction time; it declined approximately 22% after 10 h of stream operation. The roles of CO₂-based ethane dehydrogenation were also studied, where carbon dioxide can be a source of lattice oxygen and as a hydrogen consumer in reverse water-gas shift (RWGS) reaction. The effect of various catalytic factors, such as catalytic temperature, reaction time, space gas velocity, and CO₂ partial pressure on the conversion of ethane, yield, and selectivity to ethylene, were investigated as well.

Keywords: oxidative dehydrogenation; ethane; carbon dioxide; Cr-based catalyst; mesoporous organo-silica



Citation: Al-Awadi, A.S.; El-Toni, A.M.; Labis, J.P.; Khan, A.; Ghaithan, H.; Al-Zahrani, A.A.; Abasaheed, A.E.; Al-Zahrani, S.M. Mesoporous Organo-Silica Supported Chromium Oxide Catalyst for Oxidative Dehydrogenation of Ethane to Ethylene with CO₂. *Catalysts* **2021**, *11*, 642. <https://doi.org/10.3390/catal11050642>

Academic Editor: Changzhi Li

Received: 1 April 2021

Accepted: 12 May 2021

Published: 18 May 2021

Publisher's Note: MDPI stays neutral with regard to jurisdictional claims in published maps and institutional affiliations.



Copyright: © 2021 by the authors. Licensee MDPI, Basel, Switzerland. This article is an open access article distributed under the terms and conditions of the Creative Commons Attribution (CC BY) license (<https://creativecommons.org/licenses/by/4.0/>).

1. Introduction

Ethane to ethylene-based oxidative dehydrogenation (ODH) by implementing carbon dioxide as an oxidant has received much attention as a replacement to conventional thermal cracking processes and is a path for carbon dioxide utilization [1–6]. Among all investigated catalytic systems, chromium oxide supported over silica catalysts exhibits attractive catalytic performances for ODH of ethane with CO₂. It has been found that an appropriate distribution of chromium species on the support surface is a basic ingredient to obtain a superior catalytic performance [7–9]. High dispersion of chromium species leads to high concentration of reducible Cr species which are supposed to be the active phases for the dehydrogenation of alkane with CO₂ [9]. The highly dispersed Cr⁶⁺ species fully accessible to the reactant mixture have been recognized to be the active sites for light alkane dehydrogenation [10,11]. Therefore, more notice has been directed recently to siliceous mesoporous sieves, such as MCM-41 [12,13], SBA-15 [8], SBA-1 [7,10], and MSU-x [14,15] as supports for chromium-based catalytic systems. Due to their superior

BET-surface areas with uniform pore structure, siliceous mesoporous materials have been extensively investigated as chromium-dispersed materials. MCM14-supported chromium oxide, for instance, has been extensively investigated in the dehydrogenation of alkanes, and it exhibited a high Cr dispersion which was reflected positively on their catalytic performance [12,13,16]. More recently, chromium supported on ZSM-5 was found to be more effective for ethane dehydrogenation. The excellent activity results from the high dispersity and stability of CrOx species on the surface of the investigated support [5].

In 1999, a novel class of siliceous mesoporous materials, known as mesoporous organo-silica (MOS), were developed independently by three research groups: Ozin et al. [17], Inagaki et al. [18], and Stein et al. [19]. MOS is an inorganic–organic hybrid that expands the potential of using regular mesoporous materials as catalysts, adsorbents, trapping agents, etc. [9–12]. Mesoporous organo-silica is classified according to the kinds of organic groups and their position in the matrix. Terminally bonded and bridge-bonded, and either mono-functional or bifunctional are examples for these kinds of mesoporous materials. The incorporation of organic moieties into mesoporous matrix greatly changes its surface properties, such as hydrophobicity, hydrophilicity, and surface reactivity, in addition to alterations of mechanical or optical properties of these materials [20,21].

The key step of typical MOS synthesis is through the utilization of hydrolysable bridged silsesquioxanes as precursors with the supramolecular templating approach (surfactants). The precursors undergo hydrolysis, followed by poly-condensation of the silica precursors around surfactant micelles, which lead to the formation of the pore wall. Subsequent thermal treatment or extraction of the surfactant liberates the pore voids. The consistent distribution of silicon and organic atoms in the organo-silica precursors is retained in the MOS matrix, so that each individual organic group is covalently bonded to two or more silicon atoms. These bridging organic functionalities are uniformly arranged into internal pore wall as well as their outer surface, which provides them thermal and mechanical stability.

Yamada and co-workers have loaded Au nanoparticles into mesoporous organo-silica, where the developed system revealed an effective catalytic activity towards CO oxidation [22]. Karimi et al. have prepared Pd loaded on mesoporous organo-silica that showed promising efficiency for the Suzuki cross-coupling reaction [23]. The results have shown that Pd/MOS exhibited high stabilization with good selectivity for alcohol oxidation. Additionally, Karimi et al. have utilized allyl imidazolium-based mesoporous organo-silica as supports of Rh metal nanoparticles. The developed catalyst converted the secondary alcohols to the corresponding aldehyde and ketones [24]. Shylesh et al. have prepared a Cr-containing mesoporous organo-silica catalyst that was utilized for the oxidation of cyclohexane [25]. However, to the best of our knowledge, Cr-supported mesoporous organo-silica systems have not been studied for the hydrogenation catalytic reactions so far.

In this work, we have investigated MOS as a support for a chromium-containing catalytic system for ethane dehydrogenation with CO₂. A series of Cr(x)/MOS catalysts with different Cr content were synthesized and characterized with different physicochemical techniques. The catalyst behavior in the presence and absence of CO₂, and the effect of CO₂ partial pressure, were also investigated.

2. Results and Discussion

2.1. Catalyst Characterization

N₂ physisorption isotherms, along with mesopore size distribution of the prepared MOS support and Cr(x)/MOS catalysts, are illustrated in Figure 1A,B. The textural properties of synthesized samples such as BET-surface area, pore volume, and size are presented in Table 1. The physisorption isotherms display IV type profile with an H1 hysteresis loop, according to the IUPAC classification, which is a common feature of mesoporous materials. Type H1 hysteresis is associated with porous materials exhibiting pore geometry of cylindrical shape, along with pore size uniformity which is distinguished for all synthesized samples (Figure 1A). The isotherms of Cr(x)/MOS (x = 2, 5, 8, and 11 Cr wt.%)

catalysts showed that the nitrogen molecules formed multilayer adsorption. Then, capillary condensation took place in the pores of Cr(x)/MOS. As the relative pressure increases, the mesoporous nature of the MOS sample was not disturbed by chromium impregnation. Figure 1B exhibits the distribution of pore size computed by using the BJH method. All Cr(x)/MOS ($x = 2, 5, 8,$ and 11 Cr wt.%) catalysts displayed a consistently narrowing pore size distribution that peaked at 3.5 nm. According to textural properties (Table 1), both BET-surface area and total pore volume of the Cr(x)/MOS samples were reduced slightly when compared to the MOS support. This means that impregnation of MOS with Cr species caused further filling of the MOS pores with chromium oxide species.

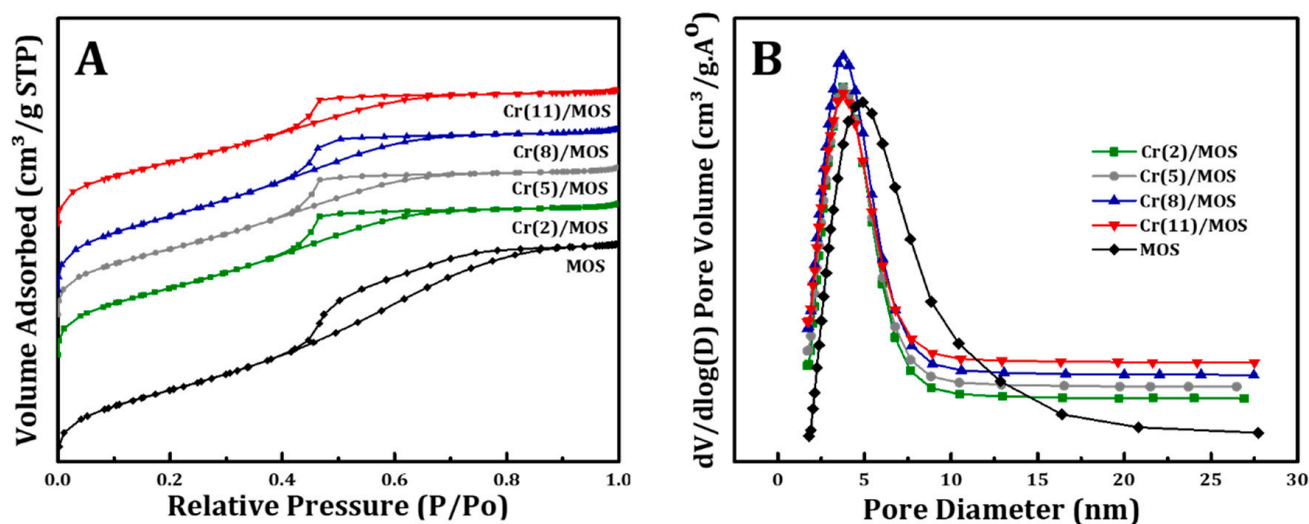


Figure 1. (A) N_2 sorption isotherms and (B) mesopore size distribution of Cr(x)/MOS catalysts prepared with varying Cr loading.

Table 1. Textural properties of the MOS and Cr(x)/MOS prepared catalysts.

Cr(x)/MOS $x =$	Cr Content wt. %	BET (m^2/g)	Pore Volume (cm^3/g)	Pore Size (nm)	Cr content by EDX wt. %	Cr surface Density (CrO_x/nm^2) ^a
MOS	0	794	0.61	4.03	-	
Cr(2)/MOS	2	695	0.49	3.50	2.55	0.33
Cr(5)/MOS	5	684	0.48	3.50	5.13	0.85
Cr(8)/MOS	8	673	0.47	3.51	7.77	1.38
Cr(11)/MOS	11	655	0.43	3.44	10.54	2.37

^a Chromium dispersion as calculated by considering the Cr content in the gel (surface density = $N_A \cdot (Cr_{Wt. \%} / Cr_{Mwt}) / S_{BET}$) [13].

The XRD patterns of the Cr(x)/MOS catalysts are illustrated in Figure 2. The diffraction peaks at $2\theta = 24.5^\circ, 33.6^\circ, 36.2^\circ, 41.5^\circ, 50.2^\circ, 54.9^\circ, 63.4^\circ,$ and 65.18° confirmed the presence of rhombohedral Cr_2O_3 crystals (JCPDS 00-006-0504) [9,13]. The intensities of the feature peaks of α - Cr_2O_3 in all prepared samples increased with increasing chromium content from 2 to 11 wt.%. The small peak intensity, as in Cr(2)/MOS, and their broadness in Cr(5)/MOS and Cr(8)/MOS samples suggested a smaller size of Cr_2O_3 crystals in these catalysts. In contrast, the Cr(11)/MOS catalyst showed higher peak intensities that could indicate the agglomeration or formation of large Cr_2O_3 particles. Generally, α - Cr_2O_3 crystals are detected over silica support at quite low Cr loading in comparison to other support systems (i.e., ZrO_2 and Al_2O_3) [11]. The low content of hydroxyl functionality within the surface of silica motivates the formation of Cr_2O_3 clusters, rather than a well-dispersed phase [11]. However, silica having a high surface area is essential in order to achieve a high dispersion of Cr species.

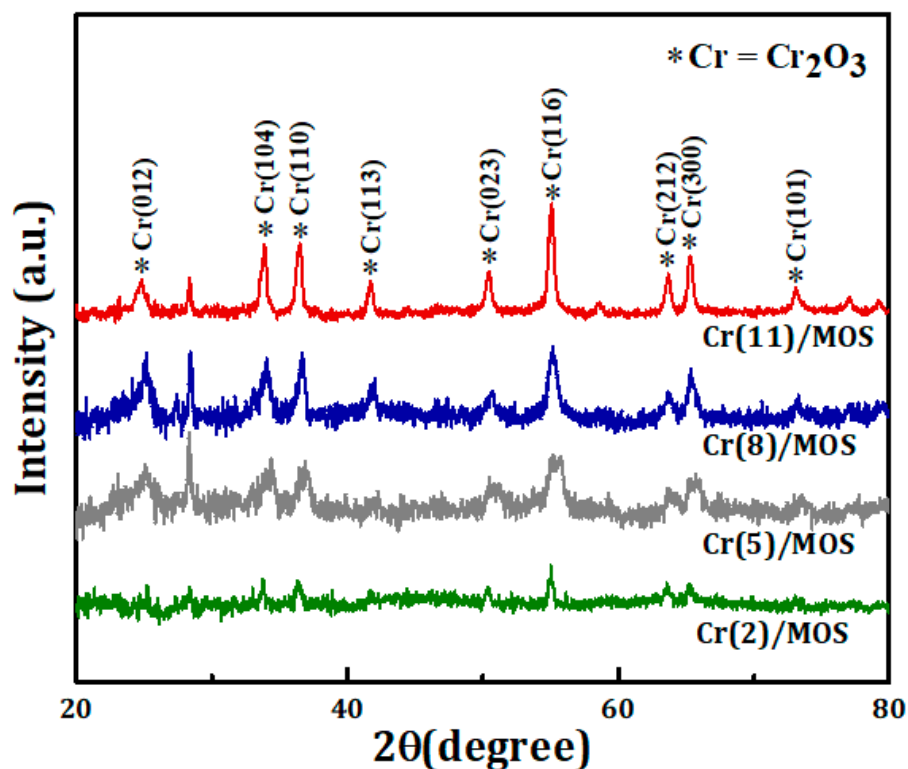


Figure 2. XRD patterns of Cr(x)/MOS catalysts prepared with varying Cr loading (*Cr = Cr₂O₃).

In order to establish more details on the surface topography of the prepared samples and to assess the dispersion of the Cr species over Cr(x)/MOS catalysts, TEM, SEM imaging, and EDX elemental mapping were obtained on MOS, Cr(2)/MOS, Cr(8)/MOS, and Cr(11)/MOS catalysts; the images are presented in Figure 3. TEM images of bare MOS (Figure 3a*) show the formation of the mesoporous organo-silica matrix. After loading of 2 wt.% of Cr (Figure 3b*), the Cr oxides had rod and cubic shapes, and their widths were in the range of 15–35 nm with good distribution onto the mesoporous organo-silica matrix. Increasing the Cr content to 8 wt.% (Figure 3c*) resulted in the formation of cubic Cr oxide nanoparticles with growth of their sizes to 50–100 nm. The state of distribution of the Cr oxide nanoparticles onto the organo-silica matrix was quite acceptable. However, increasing the loading content of Cr oxide nanoparticles to 11 wt.% (Figure 3d*) caused the formation of a mixture of rod and cubic nanoparticles with size range of 150–300 nm and poor distribution character onto the mesoporous organo-silica matrix. EDX elemental mapping also was used to investigate more about the state of distribution of CrO_x onto the mesoporous organo-silica matrix. It could be clearly observed that CrO_x species were well-dispersed on the surface of the mesoporous organo-silica support for all prepared catalysts (Figure 3a–d; CrO_x can be seen as golden color dots), and the intensity of golden dots is increasing as the chromium content increased. The Cr(11)/MOS (Figure 3d, golden) catalyst show some agglomeration of Cr species of CrO_x, as clearly seen from the larger golden dots, Cr(8)/MOS (Figure 4c, golden) possessed uniform distribution of Cr species at the catalyst surface with fine small particles. Good dispersity and the size of the metal particle are fundamental aspects governing the catalytic performance of metal-supported catalytic systems.

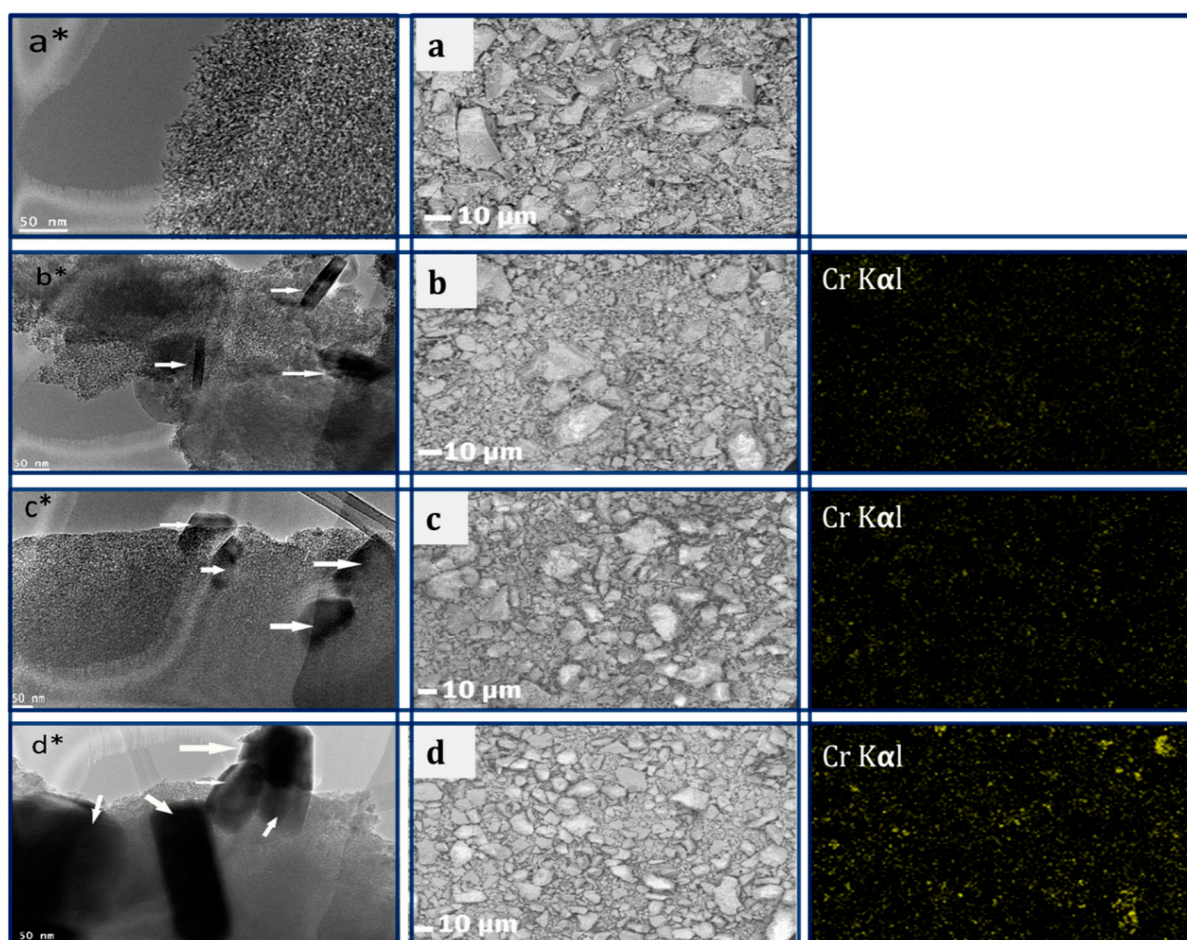


Figure 3. TEM, SEM images, and EDX elemental mapping (Cr (golden); Si (blue)) of Cr(x)/MOS catalysts prepared at different chromium loadings (a*,a) MOS; (b*,b) Cr(2)/MOS; (c*,c) Cr(8)/MOS; and (d*,d) Cr(11)/MOS (white arrows refer to Cr species).

X-ray photoelectron measurement was employed to analyze the surface chemistry and to measure the concentration of each Cr species on the synthesized samples. The XPS spectra of the Cr(x)/MOS ($x = 2, 5, 8$ and 11 wt.% Cr) samples are presented in Figure 4A,B. In order to find the ratios of various oxidation states of Cr species, the Cr2p spectra were deconvoluted and the results are given in Table 2. According to the XPS survey spectrum of the Cr(8)/MOS catalyst (Figure 4A), Cr, O, Si and C elements are present on the surface of Cr(x)/MOS catalysts. Their peaks are located at 576 (Cr 2p), 529.6(O1s), 284.6(C1s), 153(Si2s) and 103.4(Si2p) electron volts. Figure 4B displays the finely scanned XPS spectra of Cr2p of the formed catalysts. It can be observed that two intensive peaks were detected in the Cr 2p_{3/2} spectrum for all prepared samples; one at around ~577 eV, whereas the other was at ~579 eV, which can be correlated to Cr³⁺ and Cr⁶⁺, respectively [26–28]. According to the reported literature, the Cr species with high oxidation state are the main components responsible for the higher performance of Cr-based catalytic systems during the dehydrogenation of light alkanes [2,29,30]. Wang et al. suggested that the surface Cr³⁺ species and Cr⁶⁺/Cr³⁺ ratio is quite important in the ethane dehydrogenation [11], whereas Ge and his team found that the species with high oxidation states (Cr⁵⁺/Cr⁶⁺) are crucial for this reaction [31]. XPS peaks of Cr2p_{3/2} and Cr2p_{1/2} were further deconvoluted into two more peaks by using a Gaussian–Lorentzian–Voigt fitting method, considering the spin-orbit splitting of 9.3 eV and 2:1 height ratio. Based on the previous literature reports, the peaks at ~579 and ~589 eV are normally associated with the Cr⁶⁺ ions, while energies at 577, and 587 eV are ascribed to the Cr³⁺ [5,12,32,33]. It was observed that both

Cr^{6+} and Cr^{3+} had existed on the surface of all prepared samples, but with changes in their $\text{Cr}^{6+}/\text{Cr}^{3+}$ ratio. Table 2 summarizes the ratios. According to the quantitative data (Table 2), the $\text{Cr}^{6+}/\text{Cr}^{3+}$ ratio increased with the increasing Cr content up to 8 wt.% Cr, but with further a Cr increase to 11 wt.%, the ratio dropped. The Cr(8)/MOS catalyst showed the highest $\text{Cr}^{6+}/\text{Cr}^{3+}$ ratio of ~ 0.66 . The dominance of Cr^{6+} at the surface of the optimum catalyst proposes a superior catalytic conversion toward ODH of C_2H_6 with CO_2 .

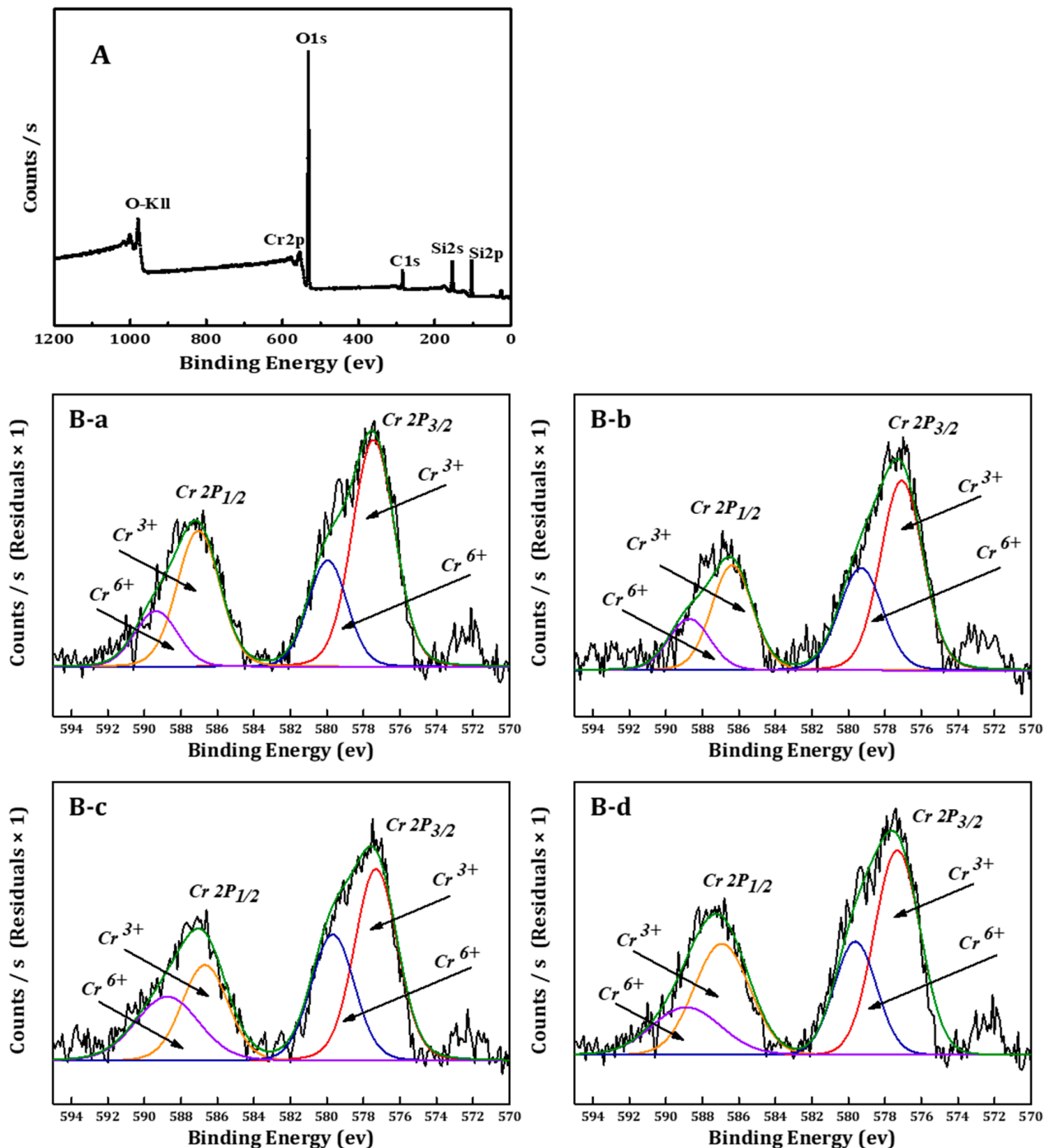
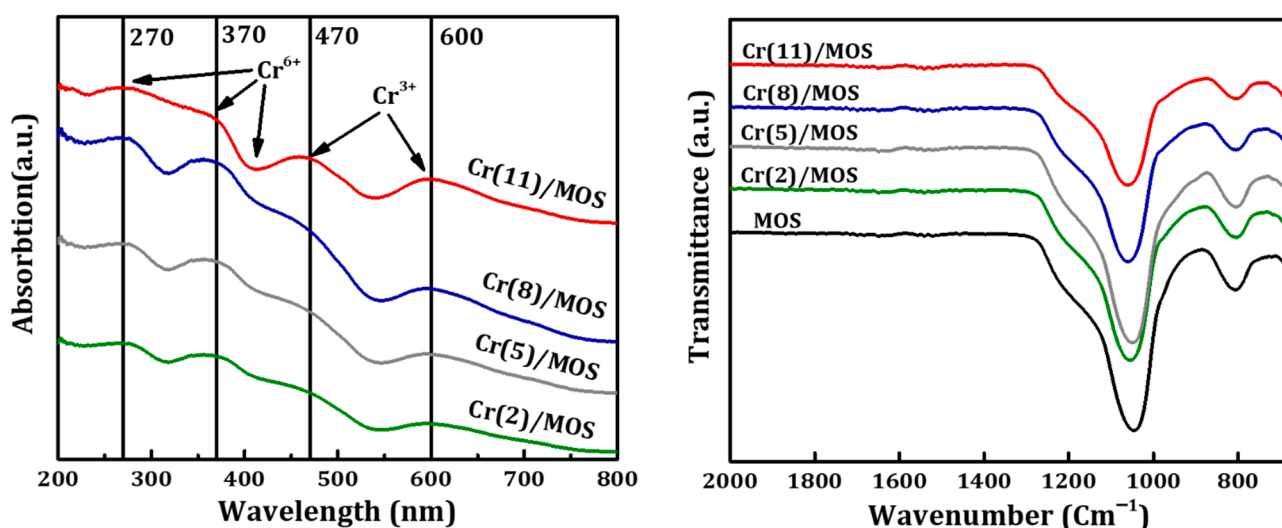


Figure 4. (A) XPS survey scan of Cr(8)/MOS; (B) Cr2p XPS spectra of Cr(x)/MOS, formed with varying Cr loading, where x: (B-a) 2, (B-b) 5, (B-c) 8, and (B-d) 11 wt.% Cr.

Table 2. XPS data of Cr(x)/MOS (x = 2, 5, 8 and 11 wt.%) catalysts.

Catalyst	Cr 2p _{3/2} Binding Energy (eV)		Cr ⁶⁺ /Cr ³⁺
	Cr ³⁺	Cr ⁶⁺	
Cr(2)/MOS	577.32	579.62	0.47
Cr(5)/MOS	577.08	579.31	0.54
Cr(8)/MOS	577.31	579.68	0.66
Cr(11)/MOS	577.32	579.62	0.55

The presence of Cr of different oxidation states was also illustrated with UV–Vis DR measurements, and the spectra are presented in Figure 5A. In all spectra, two main absorption peaks at 270 and 370 nm are detected. These two peaks are associated with charge transfer of $O^{2-} \rightarrow Cr^{6+}$ within chromate species with a tetrahedral structure [34–36]. An additional shoulder band is also observed at around 415 nm, which is attributed to dichromate or poly-chromates on the catalysts surface [26,37]. Contrastingly, the peaks at 470 and 600 nm are assigned to d-d transition of Cr³⁺ species within the octahedral structure [5,11,26,38–40]. It can be observed that the intensity of Cr⁶⁺ bands increased with increasing chromium loading up to 8 wt.%, and the Cr(8)/MOS catalyst had the highest Cr⁶⁺ bands and the lowest Cr³⁺ bands among all the prepared samples. Further increasing the chromium loading resulted in reducing the intensity of Cr⁶⁺ bands, as shown in Cr(11)/MOS catalyst, and increasing the Cr³⁺ intensities as results of Cr₂O₃ phase formation. Fourier-transform infrared spectroscopy measurements of Cr(x)/MOS catalysts were conducted in the 680–4000 cm⁻¹ range, and spectra are illustrated in Figure 5B. Silica presence in the prepared samples was confirmed by the existence of 810 and 1090 cm⁻¹ absorption bands that are assigned to symmetric vibrations of Si–O–Si bonding in the samples. Disappearance of chromium absorption bands at 905 cm⁻¹ was due to overlapping with the SiO₂ vibration band. The absorption band at about 1636 cm⁻¹ is assigned to the adsorbed water [13]. The peak observed at 2360 cm⁻¹ can be related to CO₂ which is adsorbed from the air [41,42]. It can be seen that there is no noticeable difference for the synthesized samples with various Cr content, because similar FTIR bands were detected.

**Figure 5.** UV–Vis DR spectrum (A) and FTIR patterns (B) of Cr(x)/MOS catalysts prepared with varying Cr loading.

2.2. Catalytic Performance of Cr(x)/MOS Catalysts

The catalytic activity for the formed Cr(x)/MOS samples was tested for oxidative CO₂ ethane dehydrogenation at various catalytic temperatures, and the results are displayed in Figure 6. It can be noticed that both the conversion of ethane and the yield of ethylene rapidly increased with catalytic temperature due to the endothermic character of the ODH reaction. Conversely, the selectivity of ethylene dropped slightly with catalytic temperature, suggesting that hydrocracking reactions are present at high catalytic temperatures. Moreover, the experimental results obviously showed that the Cr loading is a key element in the catalytic performance of Cr(x)/MOS catalysts. The ethane conversion as well as the ethylene yield increased significantly with increasing the chromium content of Cr(x)/MOS up to 8 wt.% Cr, and then gradually decreased with further increases in chromium content to the Cr(11)/MOS catalyst. However, this drop in activity at high Cr loading is mainly caused by the formation of less active chromium oxide crystals. The XRD, UV–Vis DRS of Cr(11)/MOS catalyst showed that the crystalline α -Cr₂O₃ is dominant in this sample. In contrast, the Cr(8)/MOS catalyst showed the highest catalytic activity for the CO₂-based ODH of ethane over the tested range of temperatures. The high activity of this catalyst could be related to superior chromium species distribution with high concentrations of reducible Cr⁶⁺ on the surface of the Cr(8)/MOS sample. It has been reported that the high concentration of reducible Cr⁶⁺ species is significant for the dehydrogenation reaction [15,40].

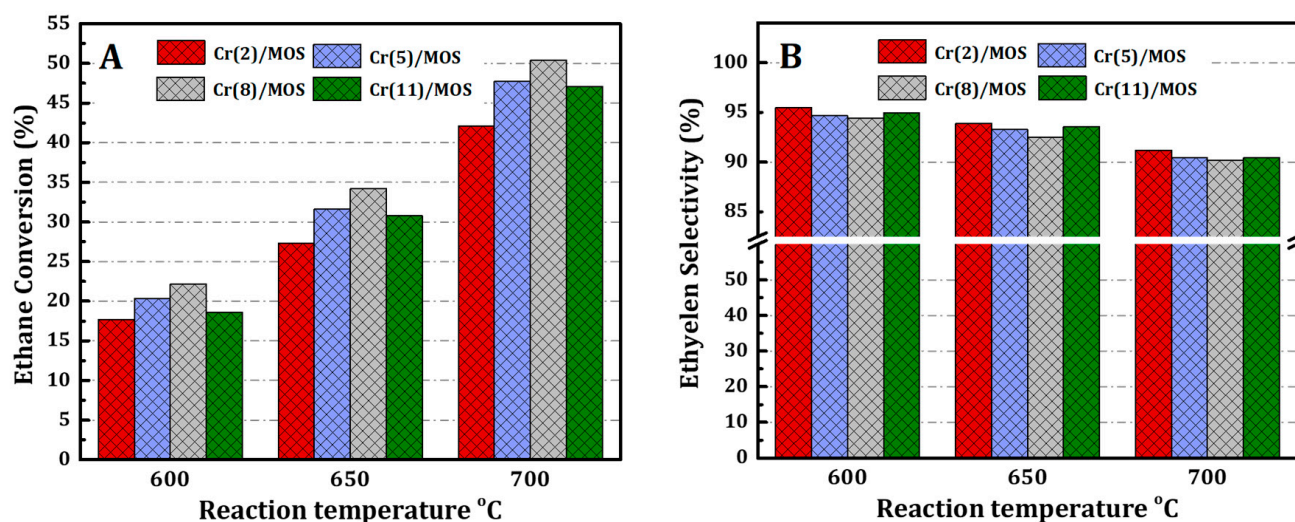


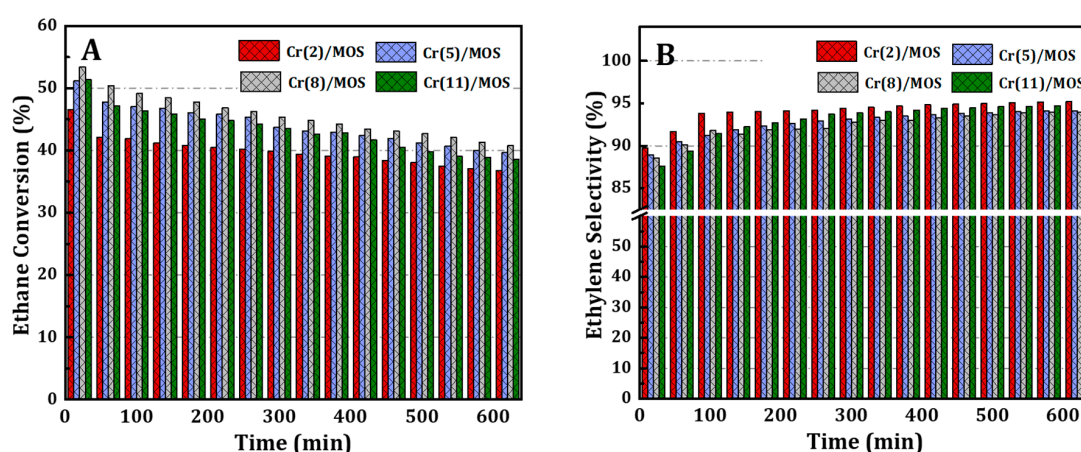
Figure 6. Effects of Cr loading on ethane conversion (A) and ethylene selectivity (B) for Cr(x)/MOS catalysts at various reaction temperatures. Reaction conditions: temperature = 700 °C; feed composition C₂H₆/CO₂/N₂ = 1/5/4; catalyst weight = 300 mg; reaction time = 1.0 h.

The SEM and XPS measurements clearly show that the Cr species were highly dispersed and Cr⁶⁺ species predominated on the prepared Cr(8)/MOS catalyst. In addition, the XPS results illustrated that the superior number of Cr⁶⁺ species and subsequently the highest Cr⁶⁺/Cr³⁺ ratio were recorded for the Cr(8)/MOS sample, which was reflected in its activity. The catalyst displayed an ethane conversion of 50.4% at 700 °C after one hour on the reaction stream and an ethylene yield of 45.4%. Table 3 summarizes the performance of some Cr-supported catalytic systems tested in the ethane dehydrogenation with CO₂, including Cr(8)/MOS prepared for this study. Although reaction conditions were diverse, Cr/MOS exhibited comparable ethane conversion and higher activity than some catalysts listed in the table, which is partly attributed to reaction conditions or the number of used catalysts. The results show that Cr/MOS is a promising active catalyst for the ODH of ethane.

Table 3. Comparison of different catalysts in the dehydrogenation of ethane with CO₂.

Catalyst	Reaction Conditions				Catalytic Activity		Ref.
	T (°C)	Flow Rate (ml/min)	Catalyst weight (g)	Feed Composition	Ethane Conversion (%)	Ethylene Selectivity (%)	
Cr(8)/MOS	700	45	0.3	C ₂ H ₆ /CO ₂ /N ₂ = 1/5/4	50.4	90.1	Present study
Cr(5)/SBA-15	700	12	0.2	C ₂ H ₆ /CO ₂ = 1/3	46.3	94.7	[8]
Cr(5)/SiO ₂	650	60	1.0	C ₂ H ₆ /CO ₂ /N ₂ = 1/5/4	56.1	92.9	[29]
Cr(5)/SiO ₂ -(SO ₄) ²⁻	650	15	1.0	C ₂ H ₆ /CO ₂ /N ₂ = 1/5/4	67.2	81.8	[33]
Cr(4)/LPMS	700	45	0.3	C ₂ H ₆ /CO ₂ /N ₂ = 1/5/4	50.5	91.1	[43]
Cr(8)/Ti(1.9)/MCM41	700	75	0.4	C ₂ H ₆ /CO ₂ /N ₂ = 1/5/4	51.9	92.8	[44]
Cr(10)-Fe(5)/ZrO ₂	650	50	0.2	C ₂ H ₆ /CO ₂ /Ar = 1/3/1	49.0	90.0	[3]
Cr(5)/CLT-IA	650	60	0.5	C ₂ H ₆ /CO ₂ /N ₂ = 1/5/4	18.9	99.5	[45]

In addition to catalytic temperature and chromium loading effects, stability of the prepared catalysts was also investigated at 700 °C for 10 h, and the results are shown in Figure 7. For all samples, the conversion of ethane and the yield of ethylene decreased slowly over catalytic time, proposing a slight de-activation of the tested catalysts. Unlike our previously [3,12,46] investigated catalytic systems, deactivation of the Cr(x)/MOS catalytic system declined approximately 22% after 10 h of on-stream operation. For instance, using large-pore mesoporous silica as a support for the chromium-based catalytic system led to the same catalytic activity (50.5% and 91.1% conversion of ethane and selectivity of ethylene, respectively), but with 39% declination in the catalytic activity for the same reaction conditions [43]. Additionally, the results of this work are comparable to those other researcher groups, indicating its importance. Shi et al., for example, tested Cr(5) /SBA-15 for ethane dehydrogenation and found that the ethane conversion dropped from 46.3 to 23.6% after reacting for 5 h [8]. In addition to coke formation, the catalyst deactivation took place basically due to the reduction of high valence states of CrO_x species, whereas the numbers of re-oxidized Cr³⁺ species were reduced with the passage of reaction time while the non-redox agglomerated Cr sites were increased. However, enhancement of the stability of Cr(x)/MOS catalysts could partly be attributed to the presence of organic components on the wall pore which may resist the agglomeration of Cr sites and inhibit catalyst sintering.

**Figure 7.** Variation of ethane conversion (A) and ethylene selectivity (B) time-on-stream over Cr(x)/MOS catalysts.

Therefore, slight deactivation of the Cr(x)/MOS catalytic system happened mostly because of the reduction of high-valence Cr⁶⁺ of CrO_x species along with coke formation. However, for better understanding of the reasons of deactivation after the reaction, characterizations of spent catalyst were compared with the fresh catalyst and the results are included as a supplementary file. Even after 10 h of on-stream operation, Cr(8)/MOS

showed high catalytic activity, with 40.81% and 38.37% for the conversion of ethane and yield of ethylene, respectively.

CO₂-based oxidative dehydrogenation of ethane over the Cr(8)/MOS catalyst was also studied at various gas hourly space velocities (GHSV), and the results are presented in Figure 8. The GHSV was altered by changing the reactant flow rate while maintaining the same reactant ratio. From the results, the conversion of ethane as well as yield of ethylene decreased, while ethylene selectivity's increased by increasing the GHSV. These results were expected because increasing the space velocity will reduce the reactants' residence time inside the catalytic system, which leads to decreases in ethane conversion. In order to clarify the role of carbon dioxide in the dehydrogenation of ethane, the catalytic reaction was conducted in the presence and absence of CO₂ over the optimum catalyst (Cr(8)/MOS) at various temperatures, and the results are presented in Figure 9.

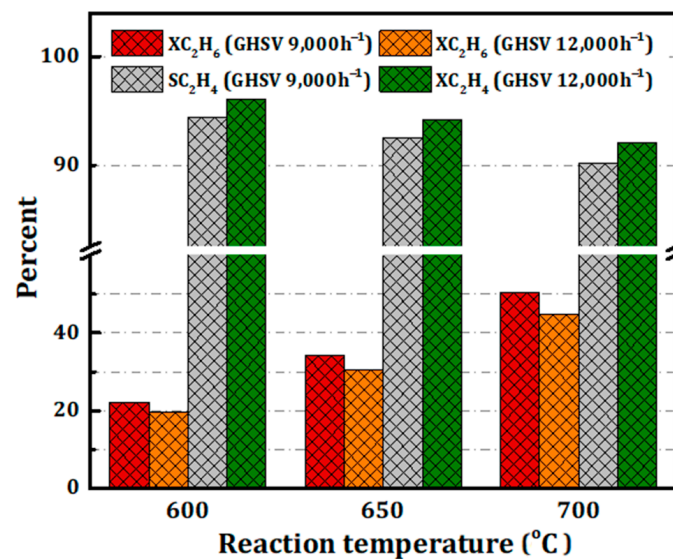


Figure 8. Effects of GHSV on the conversion of ethane and selectivity of ethylene for the Cr(8)/MOS catalyst at different temperatures.

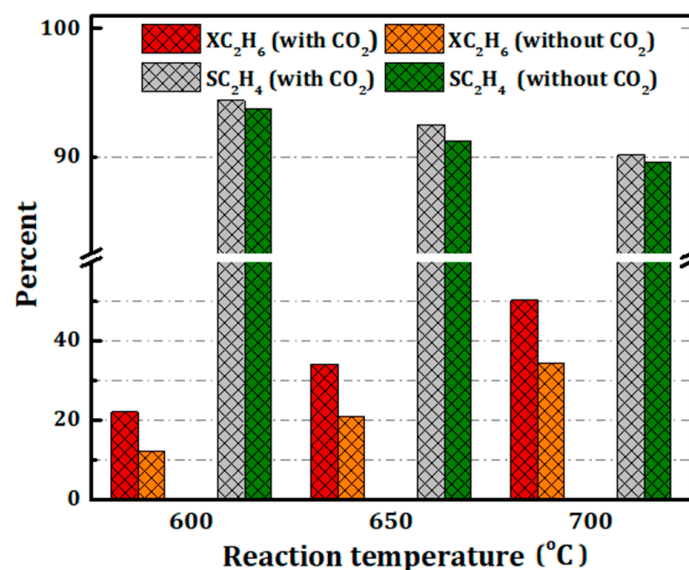
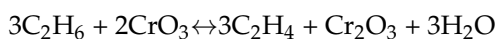


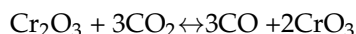
Figure 9. Effects of CO₂ addition on the conversion of ethane and selectivity of ethylene for the Cr(8)/MOS catalyst at different temperatures.

It can be observed that the catalytic performance of the Cr(8)/MOS sample increased with reaction temperature, regardless of the presence or absence of CO₂ in the reaction. Moreover, the catalytic performance of Cr(8)/MOS in the presence of CO₂ was clearly superior than that in the absence of it, revealing the enhancement effects of carbon dioxide for ethane dehydrogenation. Furthermore, ethylene selectivity was slightly improved in the presence of CO₂ as an oxidation agent. In the presence of carbon dioxide, ethylene was simultaneously formed either by dehydrogenation or oxidative dehydrogenation reactions, and a high conversion of ethane and yield of ethylene could be obtained, while the dehydrogenation of ethane without of CO₂ was thermodynamically limited [11,47]. Reaction mechanisms of ethane dehydrogenation with CO₂ over Cr-based catalysts follow the Mars–van Krevelen redox-type mechanism. This mechanism has been proposed for chromium [14,16,48–50], vanadium [51,52], manganese [53], and iron [54] oxide-based catalysts. In our catalytic system, the mechanism suggests that ethylene is simultaneously produced by the dehydrogenation and oxidative dehydrogenation of ethane [9,29,33,43,55]. According to the mechanism, oxidative dehydrogenation of ethane in the presence of CO₂ follows the following steps:

- Ethane adsorbs on Cr-species active site and/or acidic site of support;
- Adsorbed ethane reacts with lattice oxygen atoms of CrO₃ to produce both ethylene and water, and Cr³⁺, as a result of Cr⁶⁺ reduction;

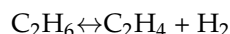


- Re-oxidation of Cr³⁺ by surface oxygen species formed by the dissociation of CO₂

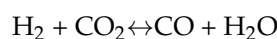


In addition to the above reactions, the following reactions occurred:

- Dehydrogenation of ethane

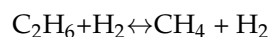


- Reverse water–gas shift (RWGS) reaction, which shifted ethane dehydrogenation towards increased ethylene production

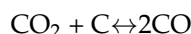


Another possible reaction is:

- Hydrocracking of ethane to methane



However, carbon dioxide could contribute either directly, by supplying the lattice oxygen in the oxidative dehydrogenation reaction, or indirectly, by removing the produced hydrogen from the dehydrogenation reaction [9]. On the other hand, the catalyst stability could be enhanced when the dehydrogenation reaction was carried out in the presence of CO₂, where it assists by removing the deposited carbon on the catalyst surface according the following equation [56]:



Eventually, the catalytic performance of the Cr/MOS catalyst in the CO₂ atmosphere was clearly higher than that in the absence of it, suggesting the stimulating role of CO₂ for the oxidative dehydrogenation of ethane in the presence of CO₂. These findings are consistent with previous studies of light alkane oxidative dehydrogenation over Cr-based catalysts [5,33,45].

Effects of the $\text{CO}_2/\text{C}_2\text{H}_6$ ratio on C_2H_6 dehydrogenation over the most active catalyst at various reaction temperatures were investigated, and the results are shown in Figure 10. It can be seen that, for all temperatures, both ethane conversion and ethylene yield increased with increasing $\text{CO}_2/\text{C}_2\text{H}_6$ ratio until it attained its peak at ratio equal to five, after which it was almost constant with further increases in the $\text{CO}_2/\text{C}_2\text{H}_6$ ratio.

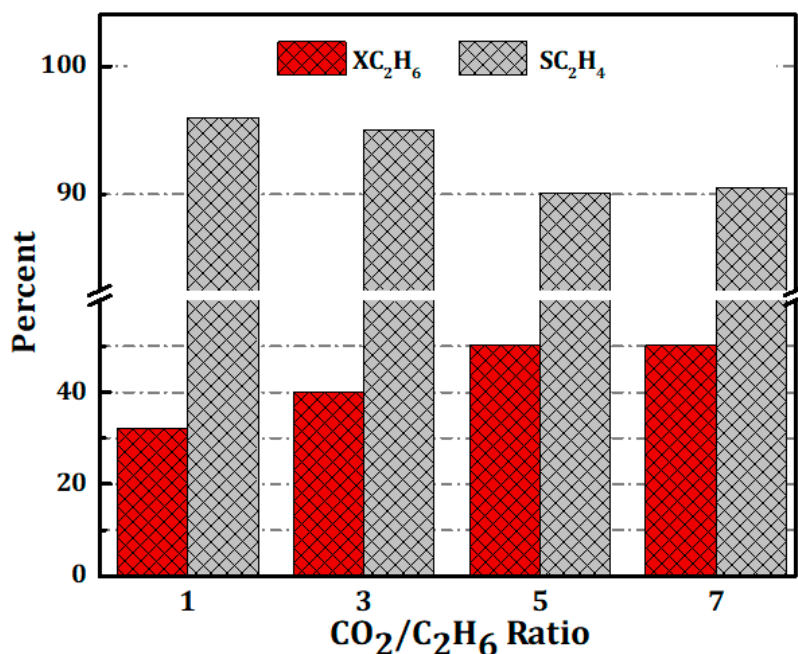


Figure 10. Effects of partial pressure of CO_2 on the conversion of ethane and selectivity of ethylene for the Cr(8)/MOS catalyst at different temperatures.

3. Materials and Methods

3.1. Materials

Compounds 1,4-bis (triethoxysilyl) benzene (BTEB), ammonium hydroxide solution NH_4OH : 28.0–30.0%, and Cetyltrimethylammonium chloride (25 wt.%) were supplied from Sigma-Aldrich (Steinheim, Germany). Chromium nitrate nonahydrate was used as a Cr precursor, and it was bought from Alfa Aesar (Karlsruhe, Germany). All chemicals were utilized as received without performing any additional purification.

3.2. Catalyst Preparation

Mesoporous organo-silica (MOS) was prepared by using BTEB and CTAC as the organo-silica source and surfactant, respectively. In a typical procedure, 4.40 ml of $\text{CH}_3(\text{CH}_2)_{15}\text{N}(\text{Cl})(\text{CH}_3)_3$, 52.5 ml of H_2O , and 4 ml of NH_4OH were combined and stirred for 10 min, in which a homogeneous solution was formed. After that, 5 ml of $\text{C}_6\text{H}_4(\text{Si}(\text{OC}_2\text{H}_5)_3)_2$ was added dropwise under vigorous stirring for 60 minutes. Then, the formed precipitate was filtered, washed, and dried overnight. The dried powder was then heat-treated at 550°C for 12 h.

In the next step, a series of Cr(x)/MOS catalysts were prepared by the incipient wetness impregnation approach where the prepared MOS support was treated with an aqueous solution having the specific amount of Cr precursor. The concentration of chromium nitrate in solution was tuned so as to obtain 2, 5, 8, and 11 wt.% of total Cr content (Cr total) in the final catalysts. The prepared samples were dried, and then were calcined at 650°C for 12 h in air. The catalysts are denoted as Cr(x)/MOS, where x stands for the nominal Cr total given in wt.% of Cr.

3.3. Catalyst Characterization

All synthesized Cr(x)/MOS samples were characterized using the same instruments mentioned in supplementary information, namely, X-ray diffraction (PANalytical X'Pert PRO MPD, PANalytical, Almelo, Netherlands), N₂ adsorption isotherms (Micromeritics ASAP 2010, Micromeritics, Norcross, GA, USA), scanning electron microscopy, energy-dispersive X-ray elemental mapping (JEOL JEM-7500F and X-ray photoelectron spectroscopy (XPS 9030 JEOL), JEOL, Tokyo, JAPAN), Fourier-transform infrared spectroscopy (Unicam 4000), and diffuse reflectance UV-Vis spectroscopy (Shmadzu, Kyoto, Japan).

3.4. Catalyst Testing

Oxidative dehydrogenation ODH reactions were performed in a stainless-steel packed catalyst bed reactor (internal diameter, 6 mm) at 600–700 °C and one atmosphere. Samples of 300 mg of Cr(x)/MOS catalysts were packed in the reactor, and glass wool was put at both ends of the catalyst bed. Prior to starting the reaction, the catalyst samples were pre-treated at 600 °C in an air atmosphere for 60 minutes before switching to the reactant mixture. During the test, the feed mixture ratio was maintained at 1:5:4 for ethane, carbon dioxide and nitrogen gases, respectively. Additionally, the total flowrate was kept at 75 mL/min. Carbon dioxide was replaced with N₂ when the experiments were implemented in the absence of CO₂. The ODH reaction was performed within a 600–700 °C temperature range. The tested samples were maintained at the reaction conditions for 20 min before starting the analysis. Both the reactants and the reaction products were analyzed by on-line Agilent 6890 N gas chromatography (Agilent 6890N, Agilent, Santa Clara,

CA, USA) which was connected to the reactor outlet. The GC was equipped with TCD and FID detectors, and using hayesep Q, molecular sieve 5 Å, and gas pro-columns.

The ethane conversion, as well as ethylene yield and selectivity, were thus computed according to Equations (1)–(3), given below:

$$\text{Ethane Conversion (\%)} = \frac{F_{\text{C}_2\text{H}_6\text{in}} - F_{\text{C}_2\text{H}_6\text{out}}}{F_{\text{C}_2\text{H}_6\text{in}}} \times 100 \quad (1)$$

$$\text{Ethylene Yield (\%)} = \frac{F_{\text{C}_2\text{H}_4}}{F_{\text{C}_2\text{H}_6\text{in}}} \times 100 \quad (2)$$

$$\text{Ethylene Selectivity (\%)} = \frac{F_{\text{C}_2\text{H}_4}}{F_{\text{C}_2\text{H}_4} + F_{\text{CH}_4}} \times 100 \quad (3)$$

where F_j is the number of moles of component j.

4. Conclusions

CO₂-based ethane oxidative dehydrogenation was studied over supported chromium oxide on mesoporous organo-silica (MOS). The results show that the prepared Cr(x)/MOS catalysts possessed promising catalytic performance in the dehydrogenation of ethane, with a less than 23% drop of its activity after 600 min. A highly active and stable catalyst Cr(8)/MOS was obtained, with an conversion of ethane ~50.9% and selectivity of ethylene ~90.1%. TEM and elemental mapping showed a gradual increment of the size of CrOx species, along with their poor distribution with increasing the Cr content. EDX analysis revealed CrOx content close to the proposed added values during the impregnation step. XPS measurements revealed that Cr⁶⁺/Cr³⁺ ratio increased with increasing the Cr content up to 8 wt.% Cr, but with a further Cr increase to 11 wt.%, the ratio dropped. The high activity of this catalyst could be related to the superior chromium species distribution with high concentration of reducible Cr⁶⁺ on the surface of the Cr(8)/MOS sample. The deactivation of the catalyst was much improved as compared to previous reports, which can be correlated to enhancement of the redox Cr species stability due to the high surface area and stable structure supports, which we developed by using MOS as a support for our catalytic system.

Supplementary Materials: The following are available online at <https://www.mdpi.com/article/10.3390/catal11050642/s1>, Figure S1: (A) N₂ sorption isotherms and (B) pore size distribution of Cr(8)/MOS catalysts before and after the reaction; Figure S2: (A) UV-Vis DR and (B) FTIR patterns of Cr(8)/MOS catalysts before and after the reaction; Figure S3: TEM images of Cr(8)/MOS catalysts (A) before and (B) after the reaction; Table S1: Textural properties of fresh and used Cr(8)/MOS catalysts.

Author Contributions: Conceptualization, writing-review editing: A.E.A. and S.M.A.-Z. Investigation, writing-original draft, and writing-review editing: A.S.A.-A., A.M.E.-T., and A.A.A.-Z. Methodology and formal analysis: A.S.A.-A., J.P.L., H.G., A.K. and A.M.E.-T. All authors have read and agreed to the published version of the manuscript.

Funding: Deanship of Scientific Research at King Saud University, Riyadh (RG-1438-094).

Data Availability Statement: The raw/processed data required to reproduce these findings cannot be shared at this time as the data also forms part of an ongoing study.

Acknowledgments: The authors extend their appreciation to the Deanship of Scientific Research at King Saud University, Riyadh for funding this work through Research Group (RG-1438-094).

Conflicts of Interest: The authors declare that they have no known competing financial interests or personal relationships that could have appeared to influence the work reported in this paper.

References

1. Wang, S.; Murata, K.; Hayakawa, T.; Hamakawa, S.; Suzuki, K. Effect of promoters on catalytic performance of Cr/SiO₂ catalysts in oxidative dehydrogenation of ethane with carbon dioxide. *Catal. Lett.* **2001**, *73*, 107–111. [[CrossRef](#)]
2. Mimura, N.; Okamoto, M.; Yamashita, H.; Oyama, S.T.; Murata, K. Oxidative Dehydrogenation of Ethane over Cr/ZSM-5 Catalysts Using CO₂ as an Oxidant. *J. Phys. Chem. B* **2006**, *110*, 21764–21770. [[CrossRef](#)] [[PubMed](#)]
3. Deng, S.; Li, S.; Li, H.; Zhang, Y. Oxidative Dehydrogenation of Ethane to Ethylene with CO₂ over Fe–Cr/ZrO₂ Catalysts. *Ind. Eng. Chem. Res.* **2009**, *48*, 7561–7566. [[CrossRef](#)]
4. Xu, L.; Liu, J.; Yang, H.; Xu, Y.; Wang, Q.; Lin, L. Regeneration behaviors of Fe/SiO₂ and Fe–Mn/SiO₂ catalysts for C₂H₆ dehydrogenation with CO₂ to C₂H₄. *Catal. Lett.* **1999**, *62*, 185–189. [[CrossRef](#)]
5. Cheng, Y.; Zhang, F.; Zhang, Y.; Miao, C.; Hua, W.; Yue, Y.; Gao, Z. Oxidative dehydrogenation of ethane with CO₂ over Cr supported on submicron ZSM-5 zeolite. *Chin. J. Catal.* **2015**, *36*, 1242–1248. [[CrossRef](#)]
6. Shi, X.; Ji, S.; Wang, K.; Li, C. Oxidative Dehydrogenation of Ethane with CO₂ over Novel Cr/SBA-15/Al₂O₃/FeCrAl Monolithic Catalysts. *Energy Fuels* **2008**, *22*, 3631–3638. [[CrossRef](#)]
7. Michorczyk, P.; Pietrzyk, P.; Ogonowski, J. Preparation and characterization of SBA-1—Supported chromium oxide catalysts for CO₂ assisted dehydrogenation of propane. *Microporous Mesoporous Mater.* **2012**, *161*, 56–66. [[CrossRef](#)]
8. Shi, X.; Ji, S.; Wang, K. Oxidative Dehydrogenation of Ethane to Ethylene with Carbon dioxide over Cr–Ce/SBA-15 Catalysts. *Catal. Lett.* **2008**, *125*, 331–339. [[CrossRef](#)]
9. Rahmani, F.; Haghghi, M.; Mahboob, S. CO₂-enhanced dehydrogenation of ethane over sonochemically synthesized Cr/clinoptilolite-ZrO₂ nanocatalyst: Effects of ultrasound irradiation and ZrO₂ loading on catalytic activity and stability. *Ultrason. Sonochem.* **2016**, *33*, 150–163. [[CrossRef](#)]
10. Michorczyk, P.; Ogonowski, J.; Niemczyk, M. Investigation of catalytic activity of Cr/SBA-1 materials obtained by direct method in the dehydrogenation of propane with CO₂. *Appl. Catal. A Gen.* **2010**, *374*, 142–149. [[CrossRef](#)]
11. Michorczyk, P.; Ogonowski, J.; Zeńczak, K. Activity of chromium oxide deposited on different silica supports in the dehydrogenation of propane with CO₂—A comparative study. *J. Mol. Catal. A Chem.* **2011**, *349*, 1–12. [[CrossRef](#)]
12. Al-Awadi, A.S.; El-Toni, A.M.; Alhoshan, M.; Khan, A.; Labis, J.P.; Al-Fatesh, A.; Abasaeed, A.E.; Al-Zahrani, S.M. Impact of precursor sequence of addition for one-pot synthesis of Cr-MCM-41 catalyst nanoparticles to enhance ethane oxidative dehydrogenation with carbon dioxide. *Ceram. Int.* **2019**, *45*, 1125–1134. [[CrossRef](#)]
13. Asghari, E.; Haghghi, M.; Rahmani, F. CO₂ Oxidative Dehydrogenation of Ethane to Ethylene over Cr/MCM-41 Nanocatalyst Synthesized via Hydrothermal/Impregnation Methods: Influence of Chromium Content on Catalytic Properties and Performance. *J. Mol. Catal. A Chem.* **2016**, *418*, 115–124. [[CrossRef](#)]
14. Liu, L.; Li, H.; Zhang, Y. Mesoporous silica-supported chromium catalyst: Characterization and excellent performance in dehydrogenation of propane to propylene with carbon dioxide. *Catal. Commun.* **2007**, *8*, 565–570. [[CrossRef](#)]
15. Baek, J.; Yun, H.J.; Yun, D.; Choi, Y.; Yi, J. Preparation of Highly Dispersed Chromium Oxide Catalysts Supported on Mesoporous Silica for the Oxidative Dehydrogenation of Propane Using CO₂: Insight into the Nature of Catalytically Active Chromium Sites. *ACS Catal.* **2012**, *2*, 1893–1903. [[CrossRef](#)]
16. Michorczyk, P.; Ogonowski, J.; Kuśtrowski, P.; Chmielarz, L. Chromium oxide supported on MCM-41 as a highly active and selective catalyst for dehydrogenation of propane with CO₂. *Appl. Catal. A Gen.* **2008**, *349*, 62–69. [[CrossRef](#)]
17. Asefa, T.; MacLachlan, M.J.; Coombs, N.; Ozin, G.A. Periodic mesoporous organosilicas with organic groups inside the channel walls. *Nature* **1999**, *402*, 867–871. [[CrossRef](#)]

18. Inagaki, S.; Guan, S.; Fukushima, Y.; Ohsuna, T.; Terasaki, O. Novel mesoporous materials with a uniform distribution of organic groups and inorganic oxide in their frameworks. *J. Am. Chem. Soc.* **1999**, *121*, 9611–9614. [[CrossRef](#)]
19. Melde, B.J.; Holland, B.T.; Blanford, C.F.; Stein, A. Mesoporous sieves with unified hybrid inorganic/organic frameworks. *Chem. Mater.* **1999**, *11*, 3302–3308. [[CrossRef](#)]
20. Mizoshita, N.; Tani, T.; Inagaki, S. Syntheses, properties and applications of periodic mesoporous organosilicas prepared from bridged organosilane precursors. *Chem. Soc. Rev.* **2011**, *40*, 789–800. [[CrossRef](#)]
21. Fujita, S.; Inagaki, S. Self-organization of organosilica solids with molecular-scale and mesoscale periodicities. *Chem. Mater.* **2008**, *20*, 891–908. [[CrossRef](#)]
22. Masatake, H.; Tetsuhiko, K.; Hiroshi, S.; Nobumasa, Y. Novel Gold Catalysts for the Oxidation of Carbon Monoxide at a Temperature far Below 0 °C. *Chem. Lett.* **1987**, *16*, 405–408.
23. Karimi, B.; Elhamifar, D.; Clark, J.H.; Hunt, A.J. Ordered Mesoporous Organosilica with Ionic-Liquid Framework: An Efficient and Reusable Support for the Palladium-Catalyzed Suzuki–Miyaura Coupling Reaction in Water. *Chem.—Eur. J.* **2010**, *16*, 8047–8053. [[CrossRef](#)] [[PubMed](#)]
24. Karimi, B.; Elhamifar, D.; Yari, O.; Khorasani, M.; Vali, H.; Clark, J.H.; Hunt, A.J. Synthesis and Characterization of Alkyl-Imidazolium-Based Periodic Mesoporous Organosilicas: A Versatile Host for the Immobilization of Perruthenate (RuO_4^-) in the Aerobic Oxidation of Alcohols. *Chem.—Eur. J.* **2012**, *18*, 13520–13530. [[CrossRef](#)] [[PubMed](#)]
25. Shylesh, S.; Srilakshmi, C.; Singh, A.; Anderson, B. One step synthesis of chromium-containing periodic mesoporous organosilicas and their catalytic activity in the oxidation of cyclohexane. *Microporous Mesoporous Mater.* **2007**, *99*, 334–344. [[CrossRef](#)]
26. Weckhuysen, B.M.; Wachs, I.E.; Schoonheydt, R.A. Surface Chemistry and Spectroscopy of Chromium in Inorganic Oxides. *Chem. Rev.* **1996**, *96*, 3327–3350. [[CrossRef](#)] [[PubMed](#)]
27. Grzybowska, B.; Słoczyński, J.; Grabowski, R.; Wcisło, K.; Kozłowska, A.; Stoch, J.; Zieliński, J. Chromium Oxide/Alumina Catalysts in Oxidative Dehydrogenation of Isobutane. *J. Catal.* **1998**, *178*, 687–700. [[CrossRef](#)]
28. Hoang, M.; Mathews, J.F.; Pratt, K.C. Oxidative Dehydrogenation of Isobutane over Supported Chromium Oxide on Lanthanum Carbonate. *J. Catal.* **1997**, *171*, 320–324. [[CrossRef](#)]
29. Wang, S.; Murata, K.; Hayakawa, T.; Hamakawa, S.; Suzuki, K. Dehydrogenation of ethane with carbon dioxide over supported chromium oxide catalysts. *Appl. Catal. A Gen.* **2000**, *196*, 1–8. [[CrossRef](#)]
30. Weckhuysen, B.M.; Schoonheydt, R.A. Alkane dehydrogenation over supported chromium oxide catalysts. *Catal. Today* **1999**, *51*, 223–232. [[CrossRef](#)]
31. Ge, X.; Zhu, M.; Shen, J. Catalytic performance of silica-supported chromium oxide catalysts in ethane dehydrogenation with carbon dioxide. *React. Kinet. Catal. Lett.* **2002**, *77*, 103–108. [[CrossRef](#)]
32. Zhao, X.; Wang, X. Oxidative dehydrogenation of ethane to ethylene by carbon dioxide over Cr/TS-1 catalysts. *Catal. Commun.* **2006**, *7*, 633–638. [[CrossRef](#)]
33. Wang, S.; Murata, K.; Hayakawa, T.; Hamakawa, S.; Suzuki, K. Oxidative dehydrogenation of ethane by carbon dioxide over sulfate-modified $\text{Cr}_2\text{O}_3/\text{SiO}_2$ catalysts. *Catal. Lett.* **1999**, *63*, 59–64. [[CrossRef](#)]
34. De Rossi, S.; Pia Casaletto, M.; Ferraris, G.; Cimino, A.; Minelli, G. Chromia/zirconia catalysts with Cr content exceeding the monolayer. A comparison with chromia/alumina and chromia/silica for isobutane dehydrogenation. *Appl. Catal. A Gen.* **1998**, *167*, 257–270. [[CrossRef](#)]
35. Zhao, X.; Wang, X. Synthesis, characterization and catalytic application of Cr-SBA-1 mesoporous molecular sieves. *J. Mol. Catal. A Chem.* **2007**, *261*, 225–231. [[CrossRef](#)]
36. Weckhuysen, B.M.; Verberckmoes, A.A.; Debaere, J.; Ooms, K.; Langhans, I.; Schoonheydt, R.A. In situ UV-Vis diffuse reflectance spectroscopy—on line activity measurements of supported chromium oxide catalysts: Relating isobutane dehydrogenation activity with Cr-speciation via experimental design. *J. Mol. Catal. A Chem.* **2000**, *151*, 115–131. [[CrossRef](#)]
37. Weckhuysen, B.M.; Verberckmoes, A.A.; Baets, A.R.D.; Schoonheydt, R.A. Diffuse Reflectance Spectroscopy of Supported Chromium Oxide Catalysts: A Self-Modeling Mixture Analysis. *J. Catal.* **1997**, *166*, 160–171. [[CrossRef](#)]
38. Ayari, F.; Mhamdi, M.; Álvarez-Rodríguez, J.; Ruiz, A.R.G.; Delahay, G.; Ghorbel, A. Selective catalytic reduction of NO with NH_3 over Cr-ZSM-5 catalysts: General characterization and catalysts screening. *Appl. Catal. B Environ.* **2013**, *367*–380. [[CrossRef](#)]
39. Cavani, F.; Koutyrev, M.; Trifirò, F.; Bartolini, A.; Ghisletti, D.; Iezzi, R.; Santucci, A.; Del Piero, G. Chemical and Physical Characterization of Alumina-Supported Chromia-Based Catalysts and Their Activity in Dehydrogenation of Isobutane. *J. Catal.* **1996**, *158*, 236–250. [[CrossRef](#)]
40. Puurunen, R.L.; Weckhuysen, B.M. Spectroscopic Study on the Irreversible Deactivation of Chromia/Alumina Dehydrogenation Catalysts. *J. Catal.* **2002**, *210*, 418–430. [[CrossRef](#)]
41. Abdollahifar, M.; Haghighi, M.; Babaluo, A.A. Syngas production via dry reforming of methane over Ni/ Al_2O_3 -MgO nanocatalyst synthesized using ultrasound energy. *J. Ind. Eng. Chem.* **2014**, *20*, 1845–1851. [[CrossRef](#)]
42. Khoshbin, R.; Haghighi, M. Urea-nitrate combustion synthesis and physicochemical characterization of CuO-ZnO- Al_2O_3 nanoparticles over HZSM-5. *Chin. J. Inorg. Chem.* **2012**, *28*, 1967–1978.
43. Al-Awadi, A.S.; Al-Zahrani, S.M.; El-Toni, A.M.; Abasaeed, A.E. Dehydrogenation of Ethane to Ethylene by CO_2 over Highly Dispersed Cr on Large-Pore Mesoporous Silica Catalysts. *Catalysts* **2020**, *10*, 97. [[CrossRef](#)]

44. Al-Awadi, A.S.; El-Toni, A.M.; Al-Zahrani, S.M.; Abasaheed, A.E.; Alhoshan, M.; Khan, A.; Labis, J.P.; Al-Fatesh, A. Role of TiO₂ nanoparticle modification of Cr/MCM41 catalyst to enhance Cr-support interaction for oxidative dehydrogenation of ethane with carbon dioxide. *Appl. Catal. A Gen.* **2019**, *584*, 117114. [[CrossRef](#)]
45. Rahmani, F.; Haghighi, M.; Amini, M. The beneficial utilization of natural zeolite in preparation of Cr/clinoptilolite nanocatalyst used in CO₂-oxidative dehydrogenation of ethane to ethylene. *J. Ind. Eng. Chem.* **2015**, *31*, 142–155. [[CrossRef](#)]
46. Al-Awadi, A.S.; El-Toni, A.M.; Alhoshan, M.; Khan, A.; Shar, M.A.; Abasaheed, A.E.; Al-Zahrani, S.M. Synergetic Impact of Secondary Metal Oxides of Cr-M/MCM41 Catalyst Nanoparticles for Ethane Oxidative Dehydrogenation Using Carbon Dioxide. *Crystals* **2019**, *10*, 7. [[CrossRef](#)]
47. Shishido, T.; Shimamura, K.; Teramura, K.; Tanaka, T. Role of CO₂ in dehydrogenation of propane over Cr-based catalysts. *Catal. Today* **2012**, *185*, 151–156. [[CrossRef](#)]
48. Nakagawa, K.; Kajita, C.; Ikenaga, N.-o.; Nishitani-Gamo, M.; Ando, T.; Suzuki, T. Dehydrogenation of light alkanes over oxidized diamond-supported catalysts in the presence of carbon dioxide. *Catal. Today* **2003**, *84*, 149–157. [[CrossRef](#)]
49. Zhang, X.; Yue, Y.; Gao, Z. Chromium Oxide Supported on Mesoporous SBA-15 as Propane Dehydrogenation and Oxidative Dehydrogenation Catalysts. *Catal. Lett.* **2002**, *83*, 19–25. [[CrossRef](#)]
50. Takehira, K.; Ohishi, Y.; Shishido, T.; Kawabata, T.; Takaki, K.; Zhang, Q.; Wang, Y. Behavior of active sites on Cr-MCM-41 catalysts during the dehydrogenation of propane with CO₂. *J. Catal.* **2004**, *224*, 404–416. [[CrossRef](#)]
51. Santacesaria, E.; Cozzolino, M.; Di Serio, M.; Venezia, A.M.; Tesser, R. Vanadium based catalysts prepared by grafting: Preparation, properties and performances in the ODH of butane. *Appl. Catal. A Gen.* **2004**, *270*, 177–192. [[CrossRef](#)]
52. Takahara, I.; Saito, M.; Inaba, M.; Murata, K. Dehydrogenation of propane over a silica-supported vanadium oxide catalyst. *Catal. Lett.* **2005**, *102*, 201–205. [[CrossRef](#)]
53. Krylov, O.V.; Mamedov, A.K.; Mirzabekova, S.R. The regularities in the interaction of alkanes with CO₂ on oxide catalysts. *Catal. Today* **1995**, *24*, 371–375. [[CrossRef](#)]
54. Michorczyk, P.; Kuśtrowski, P.; Chmielarz, L.; Ogonowski, J. Influence of redox properties on the activity of iron oxide catalysts in dehydrogenation of propane with CO₂. *React. Kinet. Catal. Lett.* **2004**, *82*, 121–130. [[CrossRef](#)]
55. Mimura, N.; Takahara, I.; Inaba, M.; Okamoto, M.; Murata, K. High-performance Cr/H-ZSM-5 catalysts for oxidative dehydrogenation of ethane to ethylene with CO₂ as an oxidant. *Catal. Commun.* **2002**, *3*, 257–262. [[CrossRef](#)]
56. Nakagawa, K.; Kajita, C.; Okumura, K.; Ikenaga, N.-o.; Nishitani-Gamo, M.; Ando, T.; Kobayashi, T.; Suzuki, T. Role of Carbon Dioxide in the Dehydrogenation of Ethane over Gallium-Loaded Catalysts. *J. Catal.* **2001**, *203*, 87–93. [[CrossRef](#)]